Epitaxial δ-Mn$_x$Ga$_{1-x}$ layers on GaN(0001): Structural, magnetic, and electrical transport properties

A. Bedoya-Pinto,[*] C. Zube, J. Malindretos,[†] A. Urban, and A. Rizzi

IV. Physikalisches Institut, Georg-August-Universität Göttingen, D-37077 Göttingen, Germany

Structural, magnetic, and electrical transport properties of δ-Mn$_x$Ga$_{1-x}$ epitaxial layers are investigated for alloy compositions in the range of $x = 0.49 \ldots 0.67$. All samples were grown by molecular beam epitaxy on GaN(0001) layers and exhibit a high-quality interface. The room-temperature saturation magnetization and the coercive field change markedly with alloy composition. An analysis of the electrical transport properties reveals that the lattice and magnon scattering contributions to the longitudinal resistivity as well as the scaling behavior of ρ_{AHE} also depend noticeably on the composition of the δ-MnGa layer. The possibility to grow δ-MnGa epitaxially on GaN(0001) over a wide range of Mn compositions and a detailed knowledge of the related physical properties are a prerequisite for the integration of this ferromagnetic alloy in wide-gap semiconductor spintronics.

I. INTRODUCTION

In the field of spintronics, great efforts are made to create spin-polarized carriers in semiconducting materials in order to combine the spin degree of freedom with the well-established optical and electrical functionality of semiconductors. One approach is doping a semiconducting host material with a few percent of magnetic ions to create a dilute magnetic semiconductor (DMS).[1] Such DMS layers can exhibit a ferromagnetic order and might be used as active device region or as spin-injecting electrodes for an adjacent normal semiconductor. However, it is still a challenge to prepare in a controlled way DMS layers which display ferromagnetic behavior at room temperature. Moreover, most of the DMS material systems under investigation are not fully understood from a theoretical point of view either.[2] An alternative approach to create spin polarization in normal semiconductors is to inject nonequilibrium spins from a ferromagnetic metal electrode. In these hybrid systems, the resistivity mismatch generally prevents an appreciable spin injection efficiency, unless the Fermi edge of the injector is almost completely spin polarized.[3] If this is not the case, an appropriate tunneling barrier between the metal electrode and the semiconductor can help to circumvent the problem. The Schottky barrier that forms at the metal/semiconductor interface can be used to tailor such a tunneling barrier if the interface is well controlled.[4,5] Furthermore, coherent tunneling might occur at high-quality crystalline interfaces. In magnetic tunnel junctions, this effect has been found to increase the magnetoresistance due to spin-selective matching of the complex band structure.[6,7] In the context of such hybrid systems, two magnetic phases of the alloy MnGa have recently gained attention for their potential in spintronic applications: the Heusler-type ferrimagnetic Mn$_3$Ga,[8–11] for which a spin polarization at the Fermi edge of 58% has been recently measured,[12] and the ferromagnetic δ-MnGa phase with AuCu-L1$_0$ structure, which is predicted to have a magnetic moment of 2.5 μ_B per Mn atom.[13] While the growth and characterization of the δ-MnGa phase has been intensively studied on GaAs,[15–17] eventually achieving spin injection at low temperatures,[18] there have been just a few reports devoted to the growth of δ-MnGa on the wide-gap semiconductor GaN.[19,20] Still, a detailed knowledge of the structural, magnetic, and electronic properties is required to aim for spin injection.

II. EXPERIMENTAL

A set of Mn$_x$Ga$_{1-x}$ epitaxial layers has been grown by plasma-assisted molecular beam epitaxy (MBE) onto Al$_2$O$_3$/GaN(0001) MOCVD templates, with the Mn concentration varying from $x = 0.39 \ldots 0.67$. High-purity Mn (5N8) and ultrahigh-purity Ga (7N+) were evaporated from conventional effusion cells in an ultrahigh vacuum chamber with a base pressure of $p = 7 \times 10^{-11}$ mbar. The composition of the films was adjusted by the control of the Mn/(Mn+Ga) ratio and confirmed by Rutherford backscattering spectrometry (RBS). The growth and surface reconstructions were monitored *in situ* by reflection high energy electron diffraction (RHEED). Crystal structures, epitaxial relationships, in- and out-of-plane lattice parameters, and interface quality were further determined by x-ray diffraction (XRD) using Cu Kα radiation and high-resolution transmission electron microscopy (HRTEM). Integral magnetic measurements were performed with a superconducting quantum interference device (SQUID) with magnetic fields up to 5 T. The magnetotransport characterization was carried out in a physical property measurement system (PPMS) within a temperature range from 2 to 400 K and magnetic fields up to 7 T.

III. RESULTS AND DISCUSSION

A. Growth and structural properties

Prior to MnGa growth, a 50 nm GaN layer was grown onto the MOCVD-GaN template at a substrate temperature of 800° C, which resulted in a (1×1) RHEED pattern typical for a smooth GaN(0001)surface. The substrate temperature was then reduced to $T_s = 250°$ C to initiate the MnGa growth. The equilibrium structure of stoichiometric Mn$_x$Ga$_{1-x}$ $(x = 0.5)$ is the tetragonal AuCu-L1$_0$ structure. A (1×1) surface reconstruction related to Mn$_x$Ga$_{1-x}$ appeared almost immediately after opening the Mn and Ga shutters, suggesting the existence of a smooth and abrupt interface. This (1×1) pattern remains
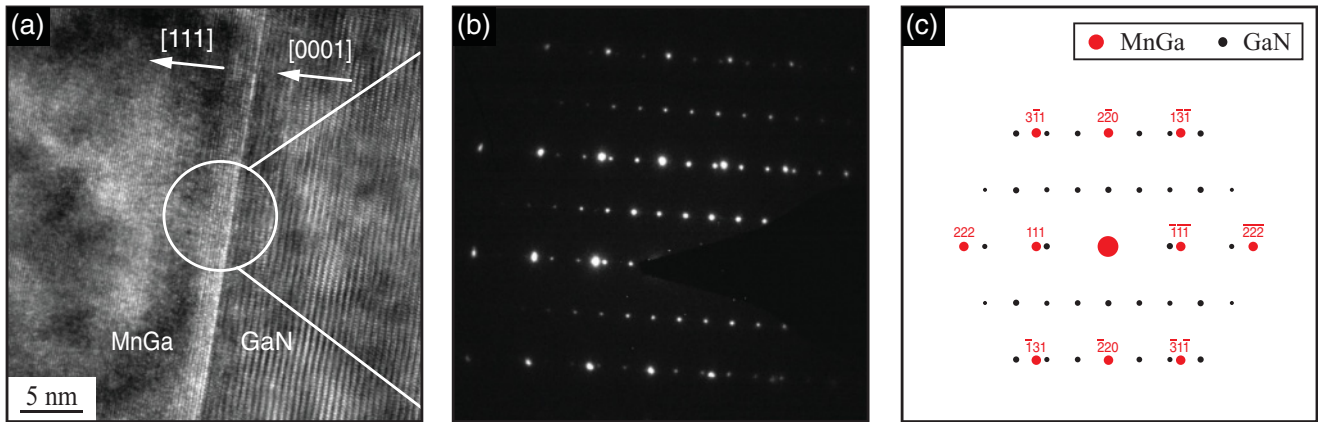
FIG. 1. (Color online) (a) Cross-sectional TEM image of the MnGa/GaN interface. (b) Selected area diffraction pattern of the interfacial region. (c) Superposition of the calculated diffraction patterns of GaN (black) and the 30° rotated MnGa (red) crystal plane, showing an excellent agreement with the SAD pattern.

streaky until the final layer thickness of $d = 150$ nm is reached. The evolution of the RHEED patterns along the [1120] and [1100] directions of the GaN template corresponds to a 30° rotation of the Mn_xGa_{1-x} hexagonal surface unit cell in the (111) plane with respect to the GaN(0001) substrate, in agreement with previous RHEED studies.[19]

High-resolution transmission electron micrographs have been acquired in cross-sectional geometry to visualize the interface properties of the layers. Figure 1(a) shows the presence of a sharp interface, in contrast to TEM images of MnGa/GaAs structures, where an amorphous layer of around 1 nm thickness is present at the interface.[18] Furthermore, the 30° rotation of the Mn_xGa_{1-x} lattice in the basal plane is confirmed by selected area diffraction (SAD). Figures 1(b) and 1(c) show a clear agreement between the SAD pattern and the calculated diffraction patterns for the 30° rotated MnGa(111) on the GaN(0001) surface. From the evaluation of both RHEED and SAD patterns, an epitaxial relationship MnGa(111)[1$\bar{1}$0] ∥ GaN(0001)[1$\bar{1}$00] and MnGa(111)[11$\bar{2}$] ∥ GaN(0001)[11$\bar{2}$0] is inferred.

The growth direction of the Mn_xGa_{1-x} layers is confirmed by XRD, revealing the Mn_xGa_{1-x}(111), GaN(0001), and Al_2O_3(0006) reflections in the same $\theta - 2\theta$ scan, as shown in Fig. 2. In addition, a 30° shift in the radial ϕ scans of the GaN(11$\bar{2}$2) with respect to the Mn_xGa_{1-x}(002) plane confirms the rotation in the basal plane between substrate and layer in the composition range $x = 0.49 \dots 0.67$. With the exception of the layer with $x = 0.39$ which corresponds to the χ-Mn_2Ga_5 phase, the Mn_xGa_{1-x} epitaxial layers crystallize in the AuCu-L1$_0$ structure. Table I summarizes the composition dependence of the lattice parameters and the full width at half maximum (FWHM) values of the (111), (200), and (002) main reflections in the $\theta - 2\theta$ and ω (rocking curve) scan modes. The evolution of the Mn_xGa_{1-x}(111) peak position with increasing Mn content corresponds to a nearly linear dependence of the d_{111} spacing on the Mn concentration x, as shown in the inset of Fig. 2. It is found that the change in the d_{111} spacing is due to the decrease of the c lattice constant of the tetragonal AuCu-L1$_0$ structure of Mn_xGa_{1-x}, while the a lattice constant remains unchanged. Regarding the crystal quality of the layers, there is a clear trend of larger FWHM

values toward higher Mn concentrations. From the width of both 2θ and ω reflections, we infer that the structural coherence length and the crystal quality decrease as the Mn/Ga ratio deviates from stoichiometry. While the AuCu-L1$_0$ structural phase seems to be stable up to $x = 0.67$, the arrangement of the excess Mn-atoms in the structure is not known, so that a comparative theoretical calculation of the electronic and magnetic properties is not straightforward.

B. Magnetic properties

The magnetic properties of the AuCu(L1$_0$)-type Mn_xGa_{1-x} epitaxially grown on GaN show two peculiar features in the studied composition range: While the saturation magnetization M_s is found to decrease with increasing Mn content, the coercive field shows the opposite trend, as depicted in Fig. 3. These observations are in agreement with previous reports of bulk MnGa[14] and of thin films of MnGa grown on
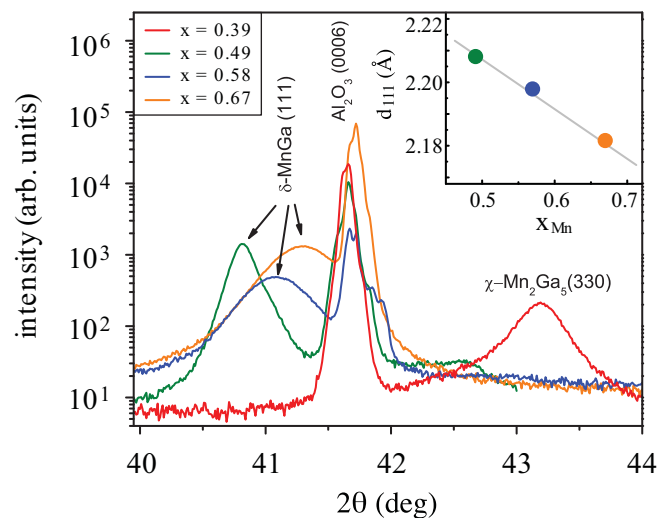
FIG. 2. (Color online) $\theta - 2\theta$ scan of Mn_xGa_{1-x} layers, confirming the [111] growth direction for $x = 0.49 \dots 0.67$ and the structural phase transition at $x = 0.39$. The inset shows the composition dependence of d_{111}.

TABLE I. Lattice parameters and FWHM values of the δ-Mn$_x$Ga$_{1-x}$ epitaxial layers.

x	d_{111} (Å)	c (Å)	a (Å)	$\Delta 2\theta_{111}$ (°)	$\Delta 2\theta_{200}$ (°)	$\Delta 2\theta_{002}$ (°)	$\Delta\omega_{111}$ (°)	$\Delta\omega_{200}$ (°)	$\Delta\omega_{002}$ (°)
0.49	2.208	3.742	3.883	0.21	0.31	0.45	0.48	1.08	0.58
0.58	2.198	3.699	3.886	0.34	0.61	1.08	0.89	1.92	–
0.67	2.186	3.659	3.886	0.47	0.64	1.45	0.87	2.19	2.21

GaAs[15–17] or GaN.[19] In general, the magnetic behavior of the Mn$_x$Ga$_{1-x}$ epitaxial layers depends not only on the alloy composition, but is also sensitive to lattice strain and crystalline orientation. Recently, Wang *et al.*[20] demonstrated that the magnetic properties of MnGa thin films can be indeed tuned by the substrate choice. In our study, the incorporation of additional Mn atoms ($x \geqslant 0.5$) simultaneously alters the strain state of the AuCu-L1$_0$ structure, as discussed in the previous section. In the literature, these two effects have been treated independently. A theoretical study by Sakuma *et al.*,[13] starting from 50% Mn, predicted that the excess Mn atoms will have an antiparallel alignment to the rest, leading to a decrease of the magnetic moment. Another theoretical work by Yang *et al.*[21] calculated the strain dependence in stoichiometric MnGa, and found that reducing the c lattice parameter leads to a smaller magnetic moment. Although the effect of the Mn incorporation and the induced strain cannot be separated in our experiments, the decrease of the magnetic moment with increasing Mn concentration and simultaneous decrease of the c lattice constant is in qualitative agreement with the trends predicted by theory.
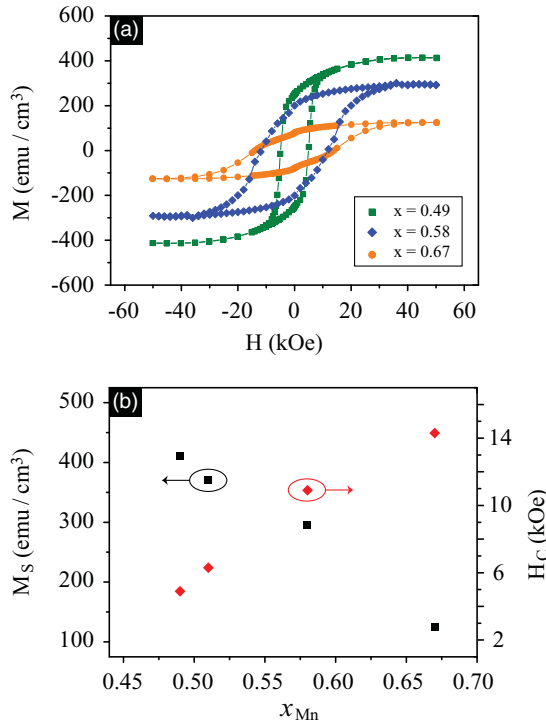
FIG. 3. (Color online) (a) Field-dependent magnetization of δ-Mn$_x$Ga$_{1-x}$ layers at 300 K. (b) Composition dependence of saturation magnetization and coercive field.

C. Electrical transport

1. Temperature dependence of the resistivity

The temperature dependence of the resistivity $\rho(T)$ of a ferromagnetic metal is, in general, sensitive to three main effects: (i) scattering at defects or impurities, described by the residual resistivity ρ_0, (ii) scattering due to electron-phonon interactions (ρ_L), and (iii) electron-spin wave scattering (ρ_m). According to Matthiessen's rule these contributions will sum up as

$$\rho = \rho_0 + \rho_L + \rho_m. \tag{1}$$

It should be noted that in $3d$ metals and alloys, as is the case of δ-Mn$_x$Ga$_{1-x}$, both s and d states are present at the Fermi level. Consequently, for both lattice (L) and magnetic (m) scattering, the conduction electrons might undergo intraband (s-s) as well as interband (s-d) transitions. The contribution due to electron-phonon scattering can be generally described as[22]

$$\rho_L = C_L \left(\frac{T}{\theta_D}\right)^n \int_0^{\Theta_D/T} \frac{x^n}{(e^x - 1)(1 - e^{-x})}dx, \tag{2}$$

where C_L is a numerical coefficient and Θ_D is the Debye temperature. The exponent in the temperature dependence in (2) is equal to $n = 5$ when considering just intraband s-s electron-phonon scattering (Bloch-Grüneisen),[22] and equal to $n = 3$ for metals with a high density of d states at the Fermi level where the conduction is determined by s-d scattering (Bloch-Wilson).[23] Above the Debye temperature Θ_D, both cases approach a linear dependence $\rho \propto T$, while for low temperatures ($T \ll \theta_D$) the temperature dependence can be well described by a T^n behavior.

The magnetic contribution to the resistivity has to be subjected to an analogous treatment. It is worth mentioning that both s-s and s-d electron-magnon scattering arise due to the exchange interaction between conduction electrons (s) and magnetic electrons ($3d$), the latter accounting for the spin-wave excitations. At low temperatures, the magnetic contribution to the resistivity is dominated by intraband s-s scattering, since interband s-d transitions require spin waves with a wave vector $\vec{k}$ larger than the distance between the Fermi surfaces of the two bands.[26] The assumption of electron scattering within a single band, which is valid at low temperatures, has been studied by Kasuya and Mannari[24,25] and results in a quadratic dependence

$$\rho_m^{s-s} = B_m^{(s-s)}T^2, \tag{3}$$

where the parameter $B_m^{(s-s)}$ is also influenced by the strength of the s-d interaction. On the other hand, at temperatures where interband scattering becomes important (usually 10 K
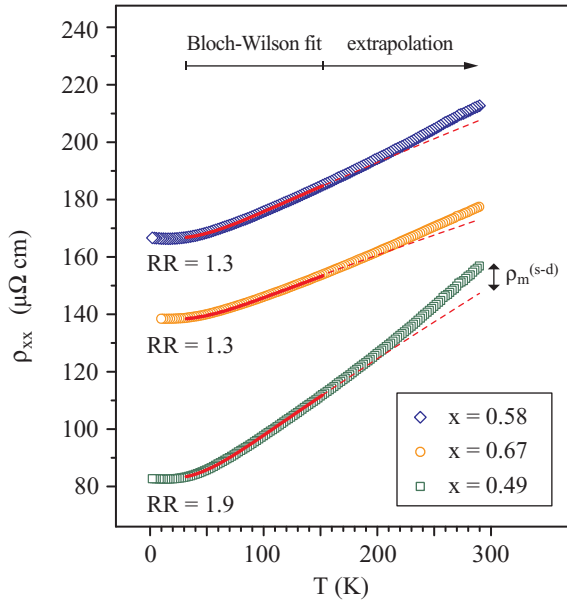
FIG. 4. (Color online) Residual resistivity ratios (RR) and temperature dependence of the resistivity in δ-Mn$_x$Ga$_{1-x}$ epitaxial layers for different Mn compositions. In the intermediate temperature range, the temperature dependence of the resistivity can be well fitted considering the lattice (Bloch-Wilson) contribution due to s-d interband scattering (solid red line). The deviation between the extrapolated Bloch-Wilson fit (dashed red line) and the measured data at higher temperatures is ascribed to the magnetic s-d scattering contribution.

$\leqslant T \leqslant 40$ K), the temperature dependence of ρ_m becomes more complicated.[26]

In order to separate the s-s and s-d scattering contributions of the lattice (ρ_L) and magnetic (ρ_m) temperature dependence of the resistivity, several temperature ranges have been separately considered, where some specific terms are expected to be dominant. In general, the s-s scattering will dominate over the s-d scattering at low temperatures, since the scattering process does not need an additional momentum Δq_{s-d} (provided by the phonon or magnon), which is required when an s electron is scattered into the d band. Accordingly, for a nonvanishing d density of states at the Fermi energy, s-d scattering might become dominant a high temperatures.

The resistivity of the δ-Mn$_x$Ga$_{1-x}$ epitaxial layers is shown in Fig. 4 as a function of Mn composition. The residual resistivity ratio RR $= \rho_{300K}/\rho_{2K}$ is a quantity which is used to analyze whether the resistance is dominated by intrinsic (phonon, magnon) or extrinsic impurity scattering, thus being

an indicator of the purity or defect density of the samples. The RR value is found to decrease with increasing Mn concentration, as listed in Table II, suggesting a high defect concentration in the nonstoichiometric samples, in agreement with the loss of crystal quality measured by x-ray diffraction. This defect formation is linked to the incorporation of excess Mn atoms ($x > 0.5$) in the AuCu-L1$_0$ structure. Thus the highest residual resistivity ratio (RR $= 1.9$) is found in the sample with $x = 0.49$ with a value that is slightly higher than the one reported for the Heusler-type Mn$_3$Ga D0$_{22}$ structure (RR $= 1.7$) grown on MgO(111) substrates.[27] Interestingly, the absolute values of the resistivity—for all temperatures—are higher for the intermediate Mn concentration ($x = 0.58$) as compared to the higher Mn concentration of $x = 0.67$, while the RR values do not differ significantly. A possible scenario which could explain this behavior is the formation of a new structure at $x = 0.67$, Mn$_2$Ga, which consists of two AuCu-L1$_0$ unit cells arranged along the c direction, with four Ga vacancies in the middle plane.[9] This crystallographic arrangement might favor the ordering in the lattice and thus reduce the scattering, leading to a decrease of ρ_0. It should be noted, however, that these similar crystal structures cannot be distinguished by x-ray diffraction measurements, since there would not be any striking effect on the lattice parameters and the epitaxial relationships due to a Mn$_2$Ga crystallographic ordering.

Regarding the temperature dependence of the resistivity, in the intermediate temperature range (30 K $\leqslant T \leqslant$ 150 K), an excellent fit was obtained considering the Bloch-Wilson expression [Eq. (2) with power $n = 3$], characteristic for phonon s-d scattering, as shown in Fig. 4. This analysis is used to derive the Debye temperature Θ_D, which does not vary much with the Mn concentration, as shown in Table II. The fact that s-d scattering processes are the main source of the resistivity in the Mn$_x$Ga$_{1-x}$ layers indicates the existence of an appreciable density of d states near the Fermi energy. At the same time, the existence of d states implies that the magnon s-d scattering contribution to the resistivity has to be taken into account. Figure 4 further shows that the Bloch-Wilson fit ($\rho_L^{(s-d)}$) of the temperature-dependent resistivity does not hold for high temperatures ($T \geqslant 150$ K). This deviation is attributed to the magnon-assisted interband scattering contribution (ρ_m^{s-d}), which has a complicated temperature dependence.[26] Although this contribution cannot be quantified, it is found that the Mn concentration has an impact on ρ_m^{s-d}. From Fig. 4, it can be inferred that the deviation from a pure phonon scattering (Bloch-Wilson fit) reaches its maximum for a stoichiometric composition ($x = 0.49$) of the δ-Mn$_x$Ga$_{1-x}$

TABLE II. Quantities derived from the temperature-dependent resistivity, taking into account intra- and interband electron transitions due to phonon and magnon scattering. The error in the coefficient $C_L^{(s-d)}$ is negligible due to the excellent accuracy of the Bloch-Wilson fit at intermediate temperatures.

x	ρ_0 ($\mu\Omega$ cm)	RR	Θ_D (K)	$B_m^{(s-s)}$ (Ω cm K^{-2})	$C_L^{(s-s)}$ (Ω cm)	$C_L^{(s-d)}$ (Ω cm)
0.49	82 ± 5	1.9	346 ± 2	$(3.5 \pm 0.4) \times 10^{-10}$	$(6.4 \pm 0.4) \times 10^{-4}$	1.64×10^{-4}
0.58	166 ± 12	1.3	362 ± 3	$(2.4 \pm 0.7) \times 10^{-10}$	$(5.2 \pm 0.8) \times 10^{-4}$	1.1×10^{-4}
0.67	138 ± 9	1.3	375 ± 3	$(1.1 \pm 0.3) \times 10^{-10}$	$(5.0 \pm 0.4) \times 10^{-4}$	0.96×10^{-4}

layers. Accordingly, by analyzing the phonon s-d scattering behavior, a stronger temperature dependence is observed for the sample near the Mn-Ga stoichiometry, which is resembled in the coefficients C_L^{s-d} obtained from the Bloch-Wilson fits as listed in Table II. These observations point to a higher density of d states at the Fermi energy for stoichiometric MnGa, which makes the s-d scattering more efficient. By increasing the Mn concentration, the s-d scattering processes become more rare, suggesting a lower density of d states at the Fermi energy. However, the Mn-concentration dependence of $N(E_F)$ is difficult to quantify, since the shape of the density of states in Mn$_x$Ga$_{1-x}$ and the position of E_F will strongly depend on the band structure, i.e., on the arrangement of the additional Mn atoms ($x \geqslant 0.5$) and the strain induced in the MnGa AuCu-L1$_0$ structure. Considering the strain effect, Yang *et al.*[21] calculated the band structure for several c lattice constants at a fixed a lattice constant value (a scenario which would correspond to our experimental observations; see Table I) and found that a higher c lattice constant results in a narrower and larger density of d states at the Fermi energy, which enhances the tendency toward ferromagnetism according to the Stoner criterion $I \times N(E_F) \geqslant 1$. However, this theoretical study was done at a fixed alloy composition (Mn$_{0.5}$Ga$_{0.5}$) and is therefore not directly comparable with our experimental scenario, even though the agreement in terms of magnetic moments and d density of states seems reasonable.

In the low temperature range ($T \leqslant 30$ K), where the intraband s-s scattering events dominate, the temperature dependence of the resistivity can be fitted using the Bloch-Grüneisen expression [Eq. (2) with power $n = 5$] for the lattice contribution (ρ_L^{s-s}) plus the magnetic contribution ($\rho_m^{s-s} \propto BT^2$). Figure 5 shows the results for the Mn$_x$Ga$_{1-x}$ layer with $x = 0.49$. The fit loses accuracy below 15 K, due to the upturn of the resistivity at very low temperatures ($T \leqslant 10$ K). This increase of the resistivity at low temperatures has been investigated in Mn$_5$Si$_3$C$_x$ metallic thin films as a function of thickness[30] and was attributed to structural disorder and scattering at grain boundaries. Indeed, for our Mn$_x$Ga$_{1-x}$ layers, this increase becomes stronger with higher Mn concentration and correlates with the structural quality
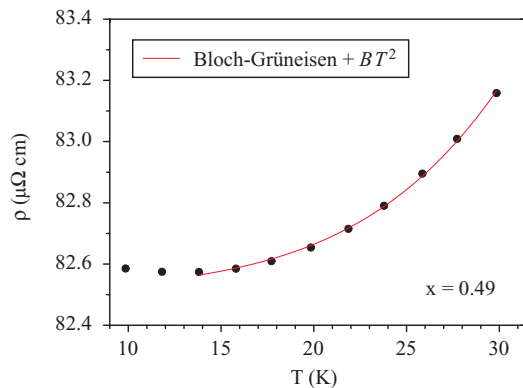
determined by x-ray diffraction (see Table I). In the considered temperature range ($15 \ldots 30$ K), the fit gives reasonable results by using the same Debye temperature Θ_D inferred from the Bloch-Wilson fits at intermediate temperatures. The various parameters obtained from the analysis of the temperature-dependent resistivity in the different temperature ranges are summarized in Table II. The Debye temperature changes slightly with Mn composition, while the coefficient $B_m^{(s-s)}$ involving magnon intraband scattering decreases with increasing Mn concentration, following the same trend as the saturation magnetization and the d density of states at the Fermi energy. Since the coefficient $B_m^{(s-s)}$ includes the strength of the interaction between the s and d electronic bands at the Fermi energy, it is plausible to assume that the s-d interaction weakens as the number of d states decreases. The coefficients C_L involving s-s and s-d phonon scattering show a slight variation with Mn composition. Although a quantitative interpretation of these coefficients appears difficult within the scattering theory in metals, they can be taken as a reference for comparison with literature values of different metals and alloys.

2. Anomalous Hall effect

Magnetic field dependent resistivity measurements in ferromagnetic metals lead to the observation of the anomalous Hall effect (AHE), commonly used to analyze spin-dependent scattering. As expected from the relation,

$$\rho_{xy} = \rho_{\mathrm{OHE}} + \rho_{\mathrm{AHE}} = R_0 H + R_s \mu_0 M, \qquad (4)$$

where ρ_{OHE} is the ordinary (linear) and ρ_{AHE} is the anomalous contribution of the transverse or Hall resistivity ρ_{xy}, the anomalous part of the resistivity is proportional to the magnetization of the sample. After subtracting the ordinary part of ρ_{xy}, we observe the same behavior of the coercive field of the $\rho_{\mathrm{AHE}}(H)$ and $M(H)$ hysteresis loops, as the Mn concentration is increased. Furthermore, the temperature dependence of the AHE has been measured from 2 K up to room temperature, as shown in Fig. 6. The magnetization is found to be independent of temperature in the investigated temperature range ($2 \ldots 300$ K), according to $M(T)$ measurements performed by SQUID

FIG. 5. (Color online) Temperature-dependent resistivity of a δ-Mn$_x$Ga$_{1-x}$ layer with $x = 0.49$. In the low temperature range, the resistivity can be fitted considering the lattice (Bloch-Grüneisen) and magnetic contributions ($\propto BT^2$), assuming intraband s-s scattering as the dominant process.
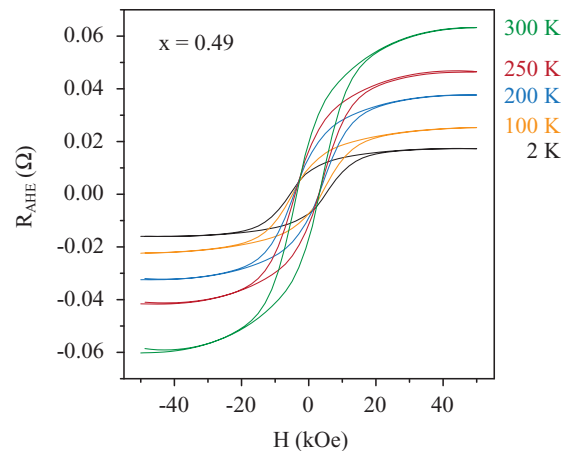
FIG. 6. (Color online) Temperature dependence of the anomalous Hall resistivity, after subtracting the linear (ordinary) term.
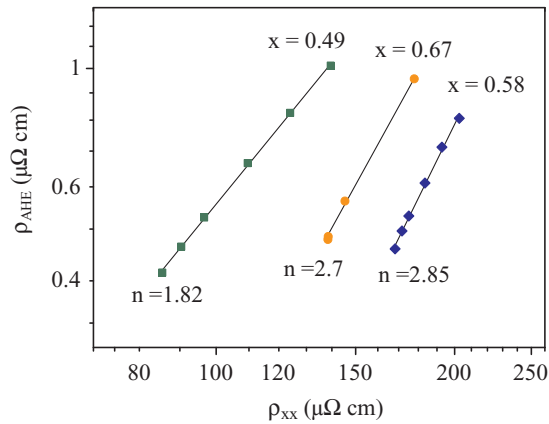
FIG. 7. (Color online) Scaling behavior of the anomalous Hall resistivity for different Mn compositions.

(not shown). Hence, the temperature dependence of ρ_{AHE} is primarily governed by the coefficient R_s.

The scaling behavior between ρ_{AHE} and the longitudinal resistivity ρ_{xx} has been widely used to identify the scattering mechanisms in ferromagnetic metals. A linear dependence ($\rho_{AHE} \propto \rho_{xx}$) is attributed to skew scattering, while a quadratic one ($\rho_{AHE} \propto \rho_{xx}^2$) is attributed to the side-jump mechanism. The former is an asymmetric scattering due to the effective spin-orbit coupling at impurity sites and is found to be dependent on the impurity concentration; the latter originates from the deflection of the electron velocity in opposite directions by the opposite electric fields experienced upon approaching and leaving an impurity.[28] An important feature of the side-jump mechanism is to be independent of the impurity concentration. A third mechanism called intrinsic contribution, which is only dependent on the band structure of the crystal and is discussed in terms of geometric concepts of Berry phase and curvature in momentum space,[28] is also proportional to ρ_{xx}^2. By analyzing the scaling behavior of ρ_{AHE} and ρ_{xx}, it is only possible to separate the skew-scattering contribution from the other two (side jump and intrinsic). A double-logarithmic plot of ρ_{AHE} against ρ_{xx} yields the exponent of the scaling behavior, which is shown in Fig. 7 for the set of δ-Mn$_x$Ga$_{1-x}$ layers with different Mn concentrations.

Near the Mn-Ga stoichiometry ($x = 0.49$), the exponent is found to be $n = 1.82$, which means that the scattering mechanism behind the AHE reveals both side-jump and intrinsic contributions. A recent review by Nagaosa et al.[28] surveyed a large number of experimental studies of the scaling behavior of the AHE and classified it in three different regimes: (i) a high-conductivity regime ($\rho_{xx} \leqslant 10^{-6}\ \Omega$ cm), in which the skew-scattering mechanism dominates; (ii) an intrinsic or scattering-independent regime ($10^{-4}\ \Omega$ cm $\geqslant \rho_{xx} \geqslant 10^{-6}\ \Omega$ cm), where $\rho_{AHE} \propto \rho_{xx}^2$; (iii) a bad metal regime ($\rho_{xx} \geqslant 10^{-4}\ \Omega$ cm), in which ρ_{AHE} increases with ρ_{xx} at a rate faster than linear ($n = 1 \ldots 2$). According to this classification, the resistivities of the δ-Mn$_x$Ga$_{1-x}$ series (80 to 200 $\mu\omega$ cm) lie at the boundary between the intrinsic and the bad metal regime, so that a scaling exponent of around $n = 2$ is expected. This is the case for the sample near the Mn-Ga stoichiometry ($x = 0.49$). As the Mn-concentration is increased ($x \geqslant 0.5$), the exponents lie between 2.7 and 2.85, as inferred from Fig. 7, values which are not expected for any classical models of spin-dependent scattering. Xiong et al.[29] reported exponents as high as $n = 3.7$ in granular Co-Ag systems and attributed the large deviation from the maximum expected scaling behavior ($n = 2$) to scattering at grain boundaries. From the structural point of view, there is a correlation between the width of the δ-Mn$_x$Ga$_{1-x}$ Bragg reflections and the Mn concentration (Fig. 2 and Table I). The structural coherence length decreases with increasing Mn concentration, hence favoring scattering at the boundaries of tilted crystal planes. Since the influence of scattering at interfaces and grain boundaries has not yet been included in the AHE theory, it is difficult to perform any further interpretation of the data.

IV. SUMMARY

In summary, the structural, magnetic, and electrical transport properties of δ-Mn$_x$Ga$_{1-x}$ epitaxial layers grown on GaN(0001) have been thoroughly characterized. The epitaxial growth with a rotation of $30°$ in the basal plane is energetically favorable at the substrate temperature of $250°$, and the AuCu-L1$_0$ crystallographic phase can be stabilized over a wide range of Mn compositions. The interface is smooth and abrupt, not showing any indication of the formation of an amorphous layer. The magnetic and magnetotransport properties are shown to depend smoothly on the alloy composition, in the range where no structural phase transition occurs. As inferred from the temperature dependence of the resistivity and the separation of the relevant scattering contributions, the excess Mn atoms and the resulting local strain influence the density of d states at the Fermi energy. This could be a handle to improve the spin polarization at E_F for using MnGa alloys as ferromagnetic electrodes for spin injection into GaN(0001) layers.

[*]Present address: CIC nanoGUNE Consolider, Tolosa Hiribidea 76, E-20018 Donostia - San Sebastian, Spain; a.bedoya@nanogune.eu

[†]malindretos@ph4.physik.uni-goettingen.de

[1]H. Ohno, Science **281**, 951 (1998).

[2]A. Zunger, S. Lany, and H. Raebiger, Physics **3**, 53 (2010).

[3]G. Schmidt, D. Ferrand, L. W. Molenkamp, A. T. Filip, and B. J. van Wees, Phys. Rev. B **62**, R4790 (2000).

[4]B. D. Schultz, N. Marom, D. Naveh, X. Lou, C. Adelmann, J. Strand, P. A. Crowell, L. Kronik, and C. J. Palmstrøm, Phys. Rev. B **80**, 201309 (2009).

[5]X. Lou, C. Adelmann, S. A. Crooker, E. S. Garlid, J. Zhang, K. S. M. Reddy, S. D. Flexner, C. J. Palmstrøm, and P. A. Crowell, Nature Phys. **3**, 197 (2007).

[6]Ph. Mavropoulos, N. Papanikolaou, and P. H. Dederichs, Phys. Rev. Lett. **85**, 1088 (2000).

[7]S. Yuasa, J. Phys. Soc. Jpn. **77**, 031001 (2008).

[8]H. Niida, T. Hori, H. Onodera, Y. Yamaguchi, and Y. Nakagawa, J. Appl. Phys. **79**, 5946 (1996).

[9]J. Winterlik, B. Balke, G. H. Fecher, C. Felser, M. C. M. Alves, F. Bernardi, and J. Morais, Phys. Rev. B **77**, 054406 (2008).

[10]F. Wu, S. Mizukami, D. Watanabe, H. Naganuma, M. Oogane, Y. Ando, and T. Miyazaki, Appl. Phys. Lett. **94**, 122503 (2009).

[11]B. Balke, G. H. Fecher, J. Winterlik, and C. Felser, Appl. Phys. Lett. **90**, 152504 (2007).

[12]H. Kurt, K. Rode, M. Venkatesan, P. S. Stamenov, and J. M. D. Coey, Phys. Rev. B **83**, 020405(R) (2011).

[13]A. Sakuma, J. Magn. Magn. Mater. **187**, 105 (1998).

[14]T. A. Bither and W. H. Cloud, J. Appl. Phys. **36**, 1501 (1965).

[15]K. Krishnan, Appl. Phys. Lett. **19**, 2365 (1992).

[16]M. Tanaka, J. P. Harbison, J. DeBoeck, T. Sands, B. Phillips, T. L. Cheeks, and V. G. Keramidas, Appl. Phys. Lett. **62**, 1565 (1993).

[17]W. Van Roy, H. Akinaga, and S. Miyanishi, Phys. Rev. B **63**, 184417 (2001).

[18]C. Adelmann, J. L. Hilton, B. D. Schultz, S. McKernan, C. J. Palmstrom, X. Lou, H. S. Chiang, and P. A. Crowell, Appl. Phys. Lett. **89**, 112511 (2006).

[19]E. Lu, D. C. Ingram, A. R. Smith, J. W. Knepper, and F. Y. Yang, Phys. Rev. Lett. **97**, 146101 (2006).

[20]K. K. Wang, E. Lu, J. W. Knepper, F. Y. Yang, and A. R. Smith, Appl. Phys. Lett. **98**, 162507 (2011).

[21]Z. Yang, J. Li, D. Wang, K. Zhang, and X. Xie, J. Magn. Magn. Mater. **182**, 369 (1998).

[22]J. M. Ziman, *Electrons and Phonons* (Clarendon, Oxford, 1960).

[23]A. H. Wilson, Proc. R. Soc. London A **167**, 580 (1938).

[24]T. Kasuya, Prog. Theor. Phys. **22**, 227 (1959).

[25]I. Mannari, Prog. Theor. Phys. **22**, 335 (1959).

[26]D. A. Goodings, Phys. Rev. **132**, 542 (1963).

[27]F. Wu, E. Sajitha, S. Mizukami, D. Watanabe, T. Miyazaki, H. Naganuma, M. Oogane, and Y. Ando, Appl. Phys. Lett. **96**, 042505 (2010).

[28]N. Nagaosa, J. Sinova, S. Onoda, A. H. MacDonald, and N. P. Ong, Rev. Mod. Phys. **82**, 1539 (2010).

[29]P. Xiong, G. Xiao, J. Q. Wang, J. Q. Xiao, J. S. Jiang, and C. L. Chien, Phys. Rev. Lett. **69**, 3220 (1992).

[30]B. Gopalakrishnan, C. Surgers, R. Montbrun, A. Singh, M. Uhlarz, and H. v. Löhneysen, Phys. Rev. B **77**, 104414 (2008).